Nonequilibrium phase transitions in extreme conditions: effects of shear flow and heat flow

1998 J. Phys.: Condens. Matter 10 11473

(http://iopscience.iop.org/0953-8984/10/49/034)

J. Phys.: Condens. Matter **10** (1998) 11473–11490. Printed in the UK PII: S0953-8984(98)96512-2

Nonequilibrium phase transitions in extreme conditions: effects of shear flow and heat flow

Akira Onuki

Department of Physics, Kyoto University, Kyoto 606, Japan

Received 5 June 1998

Abstract. Phase transitions in fluids can be drastically altered by shear flow and heat flow. We briefly discuss the mechanisms of shear effects in three very different fluids. They are near-critical fluids, semidilute polymer solutions in theta solvent, and highly supercooled liquids. As regards heat flow problems, we consider ^{4}He near the superfluid transition, which is extremely sensitive to heat flow and gravity in the vicinity of the λ-point. In particular, heat flow applied from above and gravity give rise to competing effects, producing unique nonequilibrium states, in which the temperature gradient ∇T and the transition temperature gradient $\nabla T_\lambda(p)$ under gravity cancel. (i) In a normal-fluid state, the resultant temperature difference $T - T_\lambda(p)$ can be extremely small and can even be of order 1 nK. (ii) When a superfluid region expands upward into a normal-fluid region, we conjecture that the superfluid velocity approaches a critical velocity, leading to dense generation of vortices whose role is to produce a temperature gradient equal to $\nabla T_\lambda(p)$.

1. Introduction

Fluids near phase transitions can be very sensitive to a small change of a system parameter such as the temperature or the pressure, because it can trigger phase transitions via spinodal decomposition or nucleation. There can also be a number of nonequilibrium situations in which disturbances such as shear flow, heat flow, or sound waves are applied from outside. In particular, shear flow effects have been studied extensively in various fluid systems [1]. Such effects are of great technological importance in polymeric systems. In addition we have recently started molecular dynamics simulations on nonlinear rheology in supercooled liquids [2–4]. The effect of shear in this case is very much unique and is not well known. It should be instructive to compare the mechanisms of nonlinear shear effects in the three representative cases of near-critical fluids, semidilute polymer solutions, and supercooled liquids.

Nonlinear effects of heat flow near the superfluid transition probably represent one of the most dramatic heat flow effects, though high-precision thermometry is required for such experiments [5–9]. This is because a superfluid phase exhibits only extremely small thermal resistance arising from boundary effects or quantum vortices, whereas a normal-fluid phase has a finite thermal conductivity. Furthermore, as will be discussed in this paper, it has recently been recognized that gravity in the downward direction and heat flow applied from above give rise to competing effects, and produce some surprising nonequilibrium states, either transient or steady. Because there can be other possibilities left unexplored, it should be again instructive to review these recent developments.

0953-8984/98/4911473+18$19.50

2. Nonlinear response regimes in shear flow

2.1. How can the flow field influence the critical fluctuations?

Near-critical binary fluid mixtures exhibit large-scale composition fluctuations with sizes of the order of the correlation length ξ, which grows near the critical point and easily extends to a length of the order of 10^3 Å. They undergo diffusive relaxation with the diffusion constant being given by the Einstein–Stokes formula

$$D = k_B T/6\pi\eta\xi \tag{2.1}$$

where η is the shear viscosity. The physical picture behind this is clear: the composition fluctuations are randomly convected by the velocity field fluctuations, which have magnitudes of order $v(\xi) = (k_B T/\rho\xi^3)^{1/2}$ and short lifetimes of order $\tau_v(\xi) = (\rho/\eta)\xi^2$ on the spatial scale of ξ. Then D is estimated as $v(\xi)^2\tau_v(\xi)$, leading to the above formula. The dynamics of the composition fluctuations is thus governed by the hydrodynamic interaction. The average lifetime of the composition fluctuations is enlarged as

$$\tau_\xi = \xi^2/D = 6\pi\eta\xi^3/k_B T. \tag{2.2}$$

This time can easily be of the order of 1 s in well controlled experiments. We confirm that $\tau_v(\xi) \ll \tau_\xi$.

We then naturally expect strong deformations of the fluctuations in flow field when the shear rate S exceeds τ_ξ^{-1}, which is the condition for strong shear:

$$S\tau_\xi > 1. \tag{2.3}$$

At the critical composition we have $\xi = \xi_0(T/T_c - 1)^{-\nu}$ with $\xi_0 \sim 1$ Å and $\nu = 0.63$, so we find the crossover reduced temperature:

$$\tau_s = (6\pi\eta\xi_0^3/k_B T)^{1/3\nu} S^{1/3\nu} \propto S^{0.54}. \tag{2.4}$$

There also arises a new characteristic wavenumber k_c from

$$k_c = \xi_0^{-1}\tau_s^{\nu} \propto S^{1/3}. \tag{2.5}$$

In the strong-shear regime, the fluctuations with wavenumbers larger than k_c are not much affected by the shear flow within their lifetimes and can be treated by the singular perturbation method (the dynamic renormalization group method). On the other hand, those with wavenumbers smaller than k_c are strongly affected by the shear flow before their dissipation, but their effects can be calculated by the normal perturbation method. The above procedure can be performed analytically if use is made of the ϵ-expansion method. That is, the system dimensionality d is supposed to be slightly below 4, by $\epsilon = 4 - d$.

The Fourier component $\psi_{\boldsymbol{q}}(t)$ of the composition field $\psi(\boldsymbol{r}, t)$ is governed by a linear Langevin equation at long wavelengths ($q \ll k_c$) [1, 10]:

$$\frac{\partial}{\partial t}\psi_{\boldsymbol{q}} = Sq_x \frac{\partial}{\partial q_y}\psi_{\boldsymbol{q}} - L_R q^2(r_R + q^2)\psi_{\boldsymbol{q}} + \theta_{R\boldsymbol{q}} \tag{2.6}$$

where $L_R = k_B T/6\pi\eta k_c$ ($\propto S^{-1/3}$) is the renormalized kinetic coefficient and

$$r_R = \xi_0^{-2}\tau_s^{2\nu-1}T_c^{-1}[T - T_c(S)] \tag{2.7}$$

depends on the reduced temperature linearly. That is, the critical exponent γ for strong shear is equal to the mean-field value 1. These results are obvious, because the upper cut-off wavenumber of the renormalization is given by k_c for strong shear. The critical temperature is slightly shifted downwards as $T_c(0) - T_c(S) \sim 0.1T_c\tau_s$ due to the nonlinear

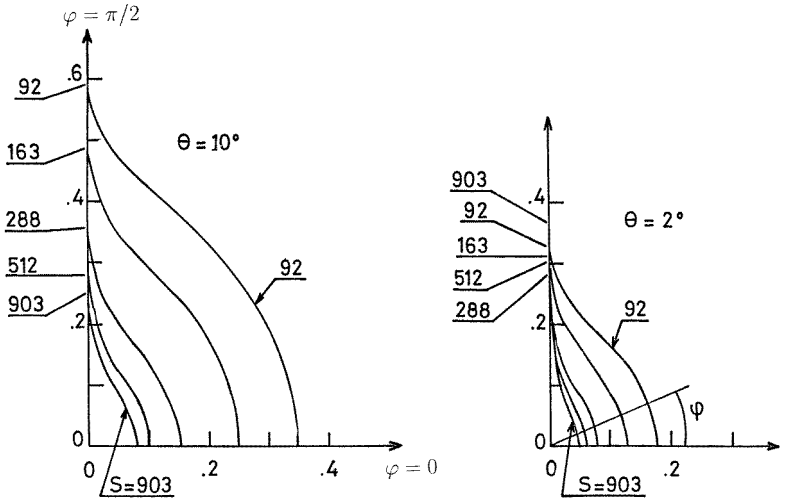

Figure 1. The reduced scattering intensity $I\boldsymbol{q})/I_{eq}(q)$ as a function of $\varphi = \tan^{-1}(q_x/q_y)$ in the polar coordinate at $T - T_c = 1.5$ mK [11]. The horizontal axis ($\varphi = 0$) is parallel to the flow ($\|\boldsymbol{x}$), while the vertical axis ($\varphi = \pi/2$) is in the velocity gradient direction. Results for two scattering angles, $\theta = 2^\circ$ ($q = 5200$ cm^{-1}) and $\theta = 10^\circ$ ($q = 26\,000$ cm^{-1}), are shown. The shear rates are $S = 903$, 512, 288, 163 and 92 s^{-1}.

hydrodynamic interaction in steady states. The random force $\theta_{R\boldsymbol{q}}$ is related to L_R via the fluctuation-dissipation relation. The steady-state structure factor $I(\boldsymbol{q}) = \langle|\psi_{\boldsymbol{q}}|^2\rangle$ satisfies

$$\left[2L_R q^2(r_R + q^2) - Sq_x \frac{\partial}{\partial q_y}\right] I(\boldsymbol{q}) = 2L_R q^2 \tag{2.8}$$

where the right-hand side arises from $\theta_{R\boldsymbol{q}}(t)$ and the Ornstein–Zernike form follows only for $q_x = 0$. We give a crude approximant extrapolating the overall anisotropic behaviours:

$$I(\boldsymbol{q}) \cong [r_R + ck_c^{8/5}|q_x|^{2/5} + q^2]^{-1} \tag{2.9}$$

where $c \cong 0.76$ and the error is less than about 20%. At small r_R ($\ll k_c^2$), $I(\boldsymbol{q}) \propto |q_x|^{-2/5}$ in most of the directions of $\boldsymbol{q}$ for $q < k_c$. This means substantial suppression of the fluctuations below the region of equilibrium critical behaviour, $I_{eq}(q) \propto 1/(\xi^{-2} + q^2)$. In figure 1 we show such behaviour of $I(\boldsymbol{q})/I_{eq}(q)$ as measured by Beysens' group for a critical mixture of aniline and cyclohexane [11].

The critical dimensionality in sheared fluids is reduced from 4 to 2.4. It is usually said that the critical behaviour acquires mean-field character for strong shear. The precise meaning of this statement is that we may linearize the dynamic equations once we have eliminated the fluctuations with wavenumbers larger than k_c in three dimensions. We should not forget of the fact that the linearized dynamic equations are still highly complex, with the coefficients nonlinearly dependent on S.

We also mention that stirring can strongly affect the critical fluctuations [12–14]. It is known that the maximum shear rate S_d in turbulence is given by $(\eta/\rho)k_d^2$, where $k_d = L_0^{-1} Re^{3/4}$ is the Kolmogorov cut-off wavenumber, L_0 being the size of the stirrer and Re being the Reynolds number, much larger than 1. In the case of near-critical fluids the composition fluctuations have sizes much shorter than the size of the smallest eddies ($\sim 1/k_d$) and are most effectively strained by the smallest eddies. These eddies turn over on the timescale of $1/S_d$, during which time the composition fluctuations are acted on by

the eddies. Experiments showed that there is no sharp phase transition in turbulence, and the scattered light intensity increases gradually but dramatically as T is lowered below T_c. As in the case of laminar shear, there is a strong-shear regime determined by $\tau_\xi S_d > 1$, in which the fluctuations are strongly suppressed by random shear.

2.2. How can shear stress induce composition fluctuations in highly viscoelastic fluids?

Effects of shear on polymeric systems are of great technological importance, but are generally very complex [1, 15]. While shear-induced mixing is usually observed, application of shear or extensional flow sometimes induces a large increase of the turbidity, indicating shear-induced composition heterogeneities or demixing, in highly viscoelastic fluid mixtures. Semidilute polymer solutions near the coexistence curve most unambiguously exhibit shear-induced demixing [16–19], where the tendency towards demixing is dramatically intensified by increase of the molecular weight M ($\gtrsim 2\times 10^6$) and the polymer volume fraction above the overlapping value.

For near-equilibrium, semidilute polymer solutions, Brochard and de Gennes noticed the presence of a long viscoelastic length ξ_{ve} [20]. That is, the relative diffusion between the polymer and the solvent on the spatial scale of ℓ takes place on the timescale of ℓ^2/D_{co}, where $D_{co} \sim k_B T/6\pi\eta_s\xi$ is the so-called cooperative diffusion constant and ξ is the correlation length (or the blob size). This time can be much shorter than the disentanglement time τ characterizing the viscoelastic relaxation, and balance of these two times gives

$$\xi_{ve} = (D_{co}\tau)^{1/2}. \tag{2.10}$$

The composition fluctuations with sizes smaller than ξ_{ve} should behave as in gels [21]. Thus the time correlation function $I_{eq}(q,t) = \langle \psi_{\boldsymbol{q}}(t)\psi_{\boldsymbol{q}}(0)^*\rangle$ of the composition fluctuations crosses over from the fluid-like behaviour to the gel-like behaviour at $q \sim \xi_{ve}^{-1}$ with increasing q.

In our shear flow problem, phase separation and viscoelastic deformations are inseparably coupled. We then need to develop a systematic dynamical theory of viscoelastic fluids treating the composition heterogeneity [22–26]. From such efforts there has arisen a new concept of a dynamical coupling between stress and diffusion. We adopt a two-fluid description to illustrate this concept below. Let the two components, 1 and 2, of the mixture be convected at the velocities $\boldsymbol{v}_1$ and $\boldsymbol{v}_1$. We consider only very slow motions, neglecting the acceleration and the temperature inhomogeneity. The equations of motion for the two components are then [24]

$$\rho_1 \frac{\partial}{\partial t}\boldsymbol{v}_1 = -\rho_1 \boldsymbol{\nabla}\mu_1 - \zeta(\boldsymbol{v}_1 - \boldsymbol{v}_2) + \boldsymbol{F}_1 \cong 0 \tag{2.11}$$

$$\rho_2 \frac{\partial}{\partial t}\boldsymbol{v}_2 = -\rho_2 \boldsymbol{\nabla}\mu_2 - \zeta(\boldsymbol{v}_2 - \boldsymbol{v}_1) + \boldsymbol{F}_2 \cong 0 \tag{2.12}$$

where ρ_1 and ρ_2 are the mass densities, μ_1 and μ_2 are chemical potentials, and ζ is the coefficient of friction between the two components. $\boldsymbol{F}_1$ and $\boldsymbol{F}_2$ are the force densities arising from the network stress $\overleftrightarrow{\boldsymbol{\sigma}}$ and the background viscosity. If the former dominate over the latter, the sum of the forces is

$$\boldsymbol{F}_1 + \boldsymbol{F}_2 \cong \boldsymbol{\nabla}\cdot \overleftrightarrow{\boldsymbol{\sigma}}\,. \tag{2.13}$$

The key question then is how the network stress is divided between the two components, on which the relative diffusion is crucially dependent. In fact, dividing (2.11) by ρ_1 and

(2.12) by ρ_2 and subtracting these equations, we obtain the relative velocity:

$$\boldsymbol{v}_1 - \boldsymbol{v}_2 = \frac{\rho_1\rho_2}{\zeta\rho}\left[-\boldsymbol{\nabla}(\mu_1 - \mu_2) + \frac{1}{\rho_1}\boldsymbol{F}_1 - \frac{1}{\rho_2}\boldsymbol{F}_2\right]. \tag{2.14}$$

In polymer solutions and gels, the network stress acts on the polymer (the component 1) and not directly on the solvent (the component 2), and it holds a one-sided stress division:

$$\boldsymbol{F}_1 \cong \boldsymbol{\nabla}\cdot\overleftrightarrow{\boldsymbol{\sigma}} \qquad \boldsymbol{F}_2 \cong \boldsymbol{0} \tag{2.15}$$

which gives

$$\boldsymbol{v}_1 - \boldsymbol{v}_2 \cong -\frac{\rho_2}{\zeta\rho}[\rho_1\,\boldsymbol{\nabla}(\mu_1 - \mu_2) - \boldsymbol{\nabla}\cdot\overleftrightarrow{\boldsymbol{\sigma}}\,]. \tag{2.16}$$

Imbalance of the network stress ($\boldsymbol{\nabla}\cdot\overleftrightarrow{\boldsymbol{\sigma}} \neq \boldsymbol{0}$) can lead to relative motion. This form of $\boldsymbol{v}_1 - \boldsymbol{v}_1$ was originally proposed by Tanaka *et al* [21] for polymer gels for analysing dynamic light scattering.

For entangled polymer blends consisting of two kinds of polymer chain, an intermediate division [24] has been proposed in the reptation scheme:

$$\boldsymbol{F}_1 = \left(\frac{\rho_1}{\rho} + \frac{\rho_1\rho_2}{\rho^2}\alpha\right)\boldsymbol{\nabla}\cdot\overleftrightarrow{\boldsymbol{\sigma}} \tag{2.17}$$

$$\boldsymbol{F}_2 = \left(\frac{\rho_2}{\rho} - \frac{\rho_1\rho_2}{\rho^2}\alpha\right)\boldsymbol{\nabla}\cdot\overleftrightarrow{\boldsymbol{\sigma}}\,. \tag{2.18}$$

The parameter α represents dynamical asymmetry, and is of the form

$$\alpha = (N_1\zeta_{01} - N_2\zeta_{02})/(\phi_1 N_1\zeta_{01} + \phi_2 N_2\zeta_{02}) \tag{2.19}$$

in terms of the polymerization indices N_1 and N_2, the monomer friction constants ζ_{01} and ζ_{02}, and the volume fractions ϕ_1 and $\phi_2 = 1 - \phi_1$. Then, for polymer blends, equation (2.14) becomes

$$\boldsymbol{v}_1 - \boldsymbol{v}_2 = -\frac{\rho_1\rho_2}{\zeta\rho^2}[\rho\,\boldsymbol{\nabla}(\mu_1 - \mu_2) - \alpha\boldsymbol{\nabla}\cdot\overleftrightarrow{\boldsymbol{\sigma}}\,]. \tag{2.20}$$

This coupling ($\alpha \neq 0$) in dynamically asymmetric mixtures can give rise to a profound influence on the dynamic scattering and phase separation [27, 28]. We give here only some of its implications for shear flow, below.

We apply shear flow to a semidilute polymer solution at a fixed volume fraction ϕ. At very long wavelengths where the timescale of the composition is longer than the viscoelastic time τ, the Fourier component of the polymer volume fraction obeys

$$\frac{\partial}{\partial t}\phi_{\boldsymbol{q}} = Sq_x\frac{\partial}{\partial q_y}\phi_{\boldsymbol{q}} - \frac{L}{1+\xi_{ve}^2 q^2}\left[q^2(r_0 + Cq^2) - \frac{2}{\phi}\frac{\partial\eta}{\partial\phi}Sq_xq_y\right]\phi_{\boldsymbol{q}} + \theta_{R\boldsymbol{q}} \tag{2.21}$$

where the coefficient r_0 decreases with lowering T, η ($\propto\tau$) is the very large solution viscosity, and $\partial\eta/\partial\phi \sim 6\eta/\phi$. It is instructive to compare the above equation with (2.6). The new aspects are as follows. First, the kinetic coefficient is dependent on q as $L/[1 + \xi_{ve}^2 q^2]$ in terms of the viscoelastic length ξ_{ve}, to which the noise term $\theta_{R\boldsymbol{q}}$ is related via the fluctuation-dissipation theorem. Second, the dynamic coupling gives rise to the very large anisotropic term ($\propto q_xq_y$) [22], leading to anisotropic fluctuation enhancement even above the coexistence curve ($r_0 > 0$). The growth of the fluctuations is maximum at $q_x = q_y$, whereas the maximum occurs for $q_x = -q_y$ in near-critical fluids under weak shear.

However, equation (2.21) should be further modified in wavenumber regions where the composition lifetime is comparable to or shorter than τ. We generally need to construct a

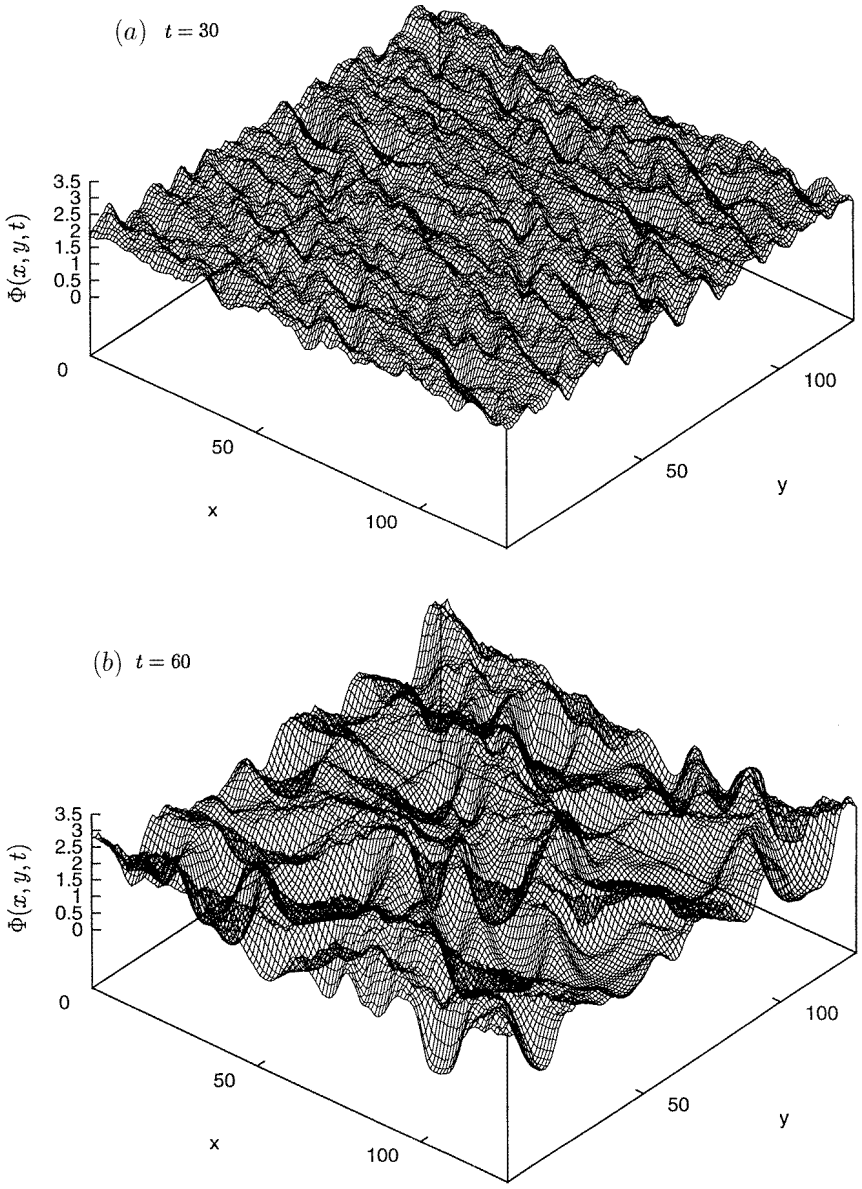

Figure 2. Snapshots of the polymer volume fraction divided by the critical value, $\Phi(x, y, t) = \phi(x, y, t)/\phi_c$, immediately after application of the shear in (a) and in a dynamically steady state in (b). Here the temperature T is at the critical temperature T_c, but the average polymer volume fraction $\langle\phi\rangle$ is double ϕ_c. The space and time are measured in units of $(5/3)^{1/2}\xi$ and $\tau_0 = (25/6)\xi^2/D_{co}$, where ξ is the correlation length and D_{co} is the cooperative diffusion constant. The solution viscosity is 13.6 times the solvent viscosity, and the stress relaxation time τ is 5.1 times τ_0.

Ginzburg–Landau scheme in which the composition and the chain deformation (which gives rise to the network stress) are coupled [1]. Although a number of experimental data have been accumulated, we give here computer simulation results of shear-induced composition

fluctuations above the coexistence curve in figure 2 [26]. Here a semidilute solution is at rest for $t < 0$ and sheared with $S = 0.25/\tau$ for $t > 0$. In an initial stage in (a), we can see the fluctuation enhancement in the direction of $q_x = q_y$. After a transient time, the system tends to a dynamically steady state as shown in (b), where the fluctuations are turbulently enhanced at various spatial scales. The fluctuation level is huge and is comparable to those in spinodal decomposition. We also observe large chaotic fluctuations of the stress [26]. See more description in the figure caption.

2.3. How can shear flow influence glassy dynamics?

Particle motions in supercooled liquids around the glass transition temperature T_g are severely restricted or jammed, giving rise to slow relaxations and highly viscoelastic behaviour characterized by the structural or α-relaxation time τ_α [29]. In glassy states, rearrangements of particle configurations or jump motions constitute elementary dynamical processes, though they are very rare events. It is also naturally expected that the rearrangements take place collectively in *clusters* whose sizes increase at low temperatures. Complexity of glassy dynamics stems from cooperativity triggered by spontaneously created disorder in an amorphous environment. Such an idea was first presented by Adam and Gibbs [30], who invented the term *cooperatively rearranging regions* (CRR). In accord with this picture, recent molecular dynamics simulations have detected spatial heterogeneities among relatively active and inactive regions in supercooled states [31, 32, 2]. Our recent work [2] on a binary mixture interacting via the soft-core potentials first characterized such patterns quantitatively; the size difference of the radii, σ_1 and σ_2, of the two components prevents crystallization. In particular, we have determined the correlation length ξ which grows as T is lowered. That is, introducing bonds between adjacent particle pairs, we have found that their breakage occurs on the timescale of τ_α, and broken bonds in an appropriately chosen time interval closely resemble the critical fluctuations in Ising spin systems.

We then consider a new nonequilibrium situation by applying a shear flow to supercooled liquids [3, 4]. We should recognize that the applied shear can induce jump motions at the rate S. Therefore, we are readily in a nonlinear regime $S\tau_\alpha > 1$, where configurational rearrangements are dominantly induced by shear, because $1/\tau_\alpha$ is the extremely small thermal jumping rate. As a result, dynamical properties in this nonlinear regime should become insensitive to the temperature, but are instead determined by S. In fact, Simmons *et al* found that the viscosity $\eta(S) = \sigma_{xy}/S$ exhibits strong, shear-thinning behaviour:

$$\eta(S) \cong \eta(0)/(1 + S\tau_\eta) \tag{2.22}$$

in soda-lime–silica glasses in steady states under shear [33], where τ_η is a long rheological time expected to be of order τ_α. Thus the shear stress σ_{xy} tends to a limiting stress ($\sim\eta(0)/\tau_\eta$) in the nonlinear regime.

Our molecular dynamics simulations in two and three dimensions are generally in agreement with the experiment [33]. In particular, we show the viscosity data in three dimensions. Figure 3(a) shows dramatic shear-thinning behaviour in the nonlinear regime where $S\tau_\alpha > 1$. Figure 3(b) demonstrates that the data can be fitted to the universal form

$$\eta(S) = A_\eta/(\tau_b(0)^{-1} + A_b S) + \eta_b \tag{2.23}$$

where $A_\eta = 0.24$, $A_b = 0.8$, and $\eta_B = 2.2$ in our model fluid in appropriate dimensionless units. $\tau_b(0)$ is a bond breakage time or a time for jump motion from cages [2–4]. We may determine the so-called α-relaxation time τ_α from the decay of the self-time-correlation function $F_s(q, t)$ from its initial value 1. That is, by setting $F_s(q, \tau_\alpha) = \mathrm{e}^{-1}$ at $q = 2\pi/\sigma_1$, we have found $\tau_\alpha \cong 0.1\tau_b$.

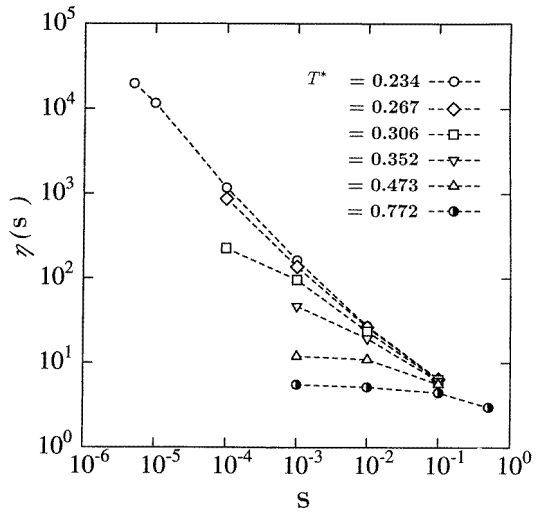

(a)

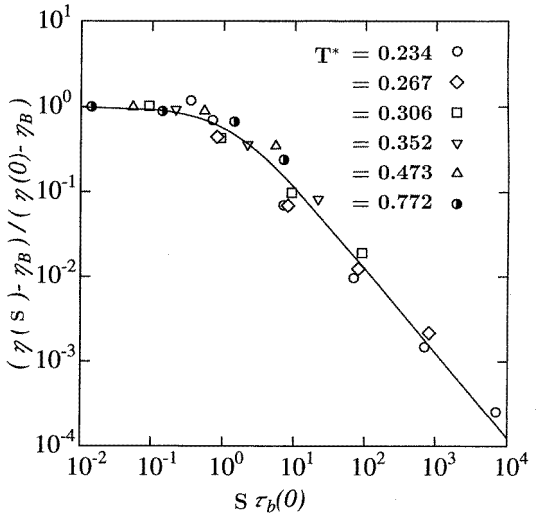

(b)

Figure 3. (a) The nonlinear shear viscosity $\eta(S) = \sigma_{xy}/S$. (b) The universal curve of $(\eta(S)-\eta_B)/(\eta(0)-\eta_B)$ versus $S\tau_b(0)$. We use a 3D supercooled binary fluid mixture interacting via the soft-core potentials, $v_{\alpha\beta}(r) = \epsilon[(\sigma_\alpha + \sigma_\beta)/2r]^{12}$, and composed of 10^4 particles. Here σ_α ($\alpha = 1, 2$) are the soft-core diameters and $T^* = k_BT/\epsilon$ is the dimensionless temperature. The shear rate and the shear viscosity are measured in units of microscopic quantities.

The above shear-thinning behaviour may be explained as follows. For each structural rearrangement a microscopic potential energy, written as ϵ, is transformed into random thermal motions of the surrounding particles. The resultant heat production rate in the nonlinear regime is estimated as

$$\dot{R} \sim n\epsilon S \tag{2.24}$$

where n is the number density. Because $\dot{R}$ is related to the viscosity by $\dot{R} = \sigma_{xy}S = \eta(S)S^2$,

we obtain $\sigma_{xy} = \eta(S)S \sim n\epsilon$, in agreement with (2.22). Thus even a very small shear can greatly accelerate the *microscopic* rearrangement processes in supercooled liquids. Interestingly, similar *jamming dynamics* has begun to be recognized also in the rheology of foams [34–36] and granular materials [37] composed of large elements. There, the thermal motions are nearly nonexistent, whereas they are overwhelming in supercooled liquids.

As a closely related problem, understanding the mechanical properties of amorphous metals such as $Cu_{57}Zr_{43}$ has been of great technological importance [38–40]. They are usually ductile in spite of their high strength. At low temperatures $T \lesssim 0.6 \sim 0.7T_g$ localized bands ($\lesssim 1$ μm), where zonal slip occurs, have been observed above a certain yield stress. At relatively high temperatures $T \gtrsim 0.6 \sim 0.7T_g$, on the other hand, shear deformations are induced *homogeneously* (on macroscopic scales) throughout samples, giving rise to viscous flow with strong, shear-thinning behaviour. In particular, in their 3D simulations Takeuchi and co-workers [40] followed atomic motions after application of a small shear strain to observe heterogeneities among *poorly and closely packed regions*, which are essentially the same entities as in the simulations of supercooled liquids [2, 4, 31, 32].

3. ^{4}He near the superfluid transition under heat flow

^{4}He near the superfluid transition is extremely sensitive to applied heat flow. The thermal conductivity in the normal-fluid phase ($T > T_\lambda$) grows as [41, 42]

$$\lambda \cong \lambda^*(T/T_\lambda - 1)^{-x_\lambda} \tag{3.1}$$

as $T \to T_\lambda$, in the linear response regime, The exponent x_λ is of order 0.44 and $\lambda^* \sim 120$ erg cm^{-1} K^{-1}. In the superfluid phase below T_λ, on the other hand, a thermal counterflow is produced in the heat flow direction, in which there is no net mass current ($\rho_s v_s + \rho_n v_n = 0$) but the normal-fluid component carries heat ($Q = \rho s T v_n$) without there being appreciable mutual interaction between the two components. A very small thermal resistance arises from quantum vortices, however. Here $\rho_s \propto (1 - T/T_\lambda)^\nu$ ($\nu = 2/3$), $\rho_n = \rho - \rho_s$, v_s, and v_n are the densities and velocities of the superfluid and normal-fluid components, respectively. ρ and s are the mass density and entropy per unit mass. In this geometry, at the two ends of the cell, phase conversion between the two components takes place and small temperature jumps are produced (the Kapitza boundary resistance).

3.1. A He I–He II interface

It is natural to expect nonlinear response regimes with respect to heat flux Q very close to T_λ [5–8]. In particular, we may consider a situation in which the temperature at one end of the cell is above T_λ and that at the other end is slightly below T_λ. The temperature in the cooler side should be nearly constant because of the thermal counterflow, whereas it has a much larger gradient on the normal-fluid side. Then a He I–He II interface emerges separating the two phases, across which the temperature gradient is discontinuous. This interface is very much a unique nonequilibrium object. It always appears when ^{4}He in a normal-fluid state is cooled from the boundary below T_λ or when ^{4}He in a superfluid state is warmed from the boundary above T_λ.

Let us discuss the interface structure using some scaling arguments [5]. On the superfluid side the correlation length is given by $\xi = \xi_{0-}\tau_\infty^{-\nu}$ where $\xi_{0-} \sim 1$ Å is a microscopic length, $\nu = 2/3$ is the usual critical exponent, and $\tau_\infty = 1 - T/T_\lambda$ is the reduced temperature. The complex order parameter ψ depends sinusoidally on the coordinate x in the heat flow

direction as $\exp(-\mathrm{i}kx)$, where $k = mv_s/\hbar$ in terms of the ^{4}He mass m and the superfluid velocity v_s. The heat flux Q is expressed as

$$Q = \rho s T |v_n| \cong s T \rho_s |v_s| = (\hbar s T/m)\rho_s k. \tag{3.2}$$

Here v_s should be smaller than a critical value:

$$v_{sc} = \hbar/(\sqrt{3} m\xi). \tag{3.3}$$

Flow-carrying states in which a complex order parameter behaves as $\exp(\mathrm{i}kx)$ become unstable for $k\xi > 1/\sqrt{3}$ against long-wavelength perturbations of the phase [43, 44]. (This is generally called the Eckhaus instability in nonlinear dynamics [45].) As a theoretical estimate indicated [5], $k\xi$ in the two-phase coexistence is smaller than but of the same order as $1/\sqrt{3}$. Thus, the two-phase structure is stable theoretically. However, it is much larger than a threshold value of 0.036, above which vortex nucleation becomes appreciable near T_λ [46]. Therefore, we expect a considerable amount of vortices on the superfluid side. As a rough estimate we set $k \sim \xi^{-1}$ in (3.2) to obtain

$$\tau_\infty \sim (m\xi_{0-}/\hbar s T \rho_s^*)^{3/4} Q^{3/4} \tag{3.4}$$

where we have set $\rho_s = \rho_s^*(1 - T/T_\lambda)^{2/3}$. The coefficient in front of $Q^{3/4}$ is of order 10^{-8} with Q in erg cm^{-2} s^{-1}. The correlation length is

$$\xi \sim (\hbar s T \rho_s^* \xi_{0-}/m)^{1/2} Q^{-1/2} \tag{3.5}$$

with the coefficient of order 3×10^{-3} in cgs units.

We may also discuss the structure using scaling arguments on the normal-fluid side. That is, a characteristic reduced temperature τ_Q and length ξ_Q may be introduced by the heat conduction relation

$$Q \sim (\lambda^* \tau_Q^{-x_\lambda})(T_\lambda \tau_Q/\xi_Q) \tag{3.6}$$

and the correlation length relation

$$\xi_Q = \xi_{0+}\tau_Q^{-2/3}$$

above T_λ with $\xi_{0+} \sim 1$ Å. Then,

$$\tau_Q \sim (Q\xi_{0+}/T_\lambda \lambda^*)^{1/(1+\nu-x_\lambda)} \tag{3.7}$$

$$\xi_Q \sim \xi_{0+}(Q\xi_{0+}/T_\lambda \lambda^*)^{-\nu/(1+\nu-x_\lambda)}. \tag{3.8}$$

These quantities are slightly different from τ_∞ and ξ in (3.4) and (3.5) because $x_\lambda > 1/3$, but they are numerically of the same order. The interface thickness is of order ξ in (3.5) or ξ_Q in (3.8). Unless Q is very small, it is very thin compared with characteristic sizes of thermometers. If Q is made very small ($\lesssim$1 erg cm^{-2} s^{-1}), the interface structure is determined by gravity on the Earth as will be discussed below (3.18).

The interface profile can be calculated approximately or numerically on the basis of a time-dependent Ginzburg–Landau model [47, 48]. It is known that the complex order parameter and the temperature (or the entropy) constitute a closed set of dynamic equations near the λ-point (the F model [48]). Here we make them dimensionless by appropriate scalings [5]:

$$\frac{\partial}{\partial t}\Psi = \mathrm{i}a^{-1}A\Psi - \Gamma\left[A - \nabla^2 + |\Psi|^2\right]\Psi \tag{3.9}$$

$$\frac{\partial}{\partial t}\left(A - \frac{1}{2}a^2|\Psi|^2\right) = a\boldsymbol{\nabla}\cdot\boldsymbol{J}_s + \boldsymbol{\nabla}\cdot\lambda\,\boldsymbol{\nabla}A \tag{3.10}$$

where a ($\sim$1) is a positive constant, and Γ (=complex) and λ are the dimensionless kinetic coefficients expected to be of order 1 (in the same notation as for the original thermal conductivity). In the dimensionless forms, Ψ is the complex order parameter, A is the reduced temperature, and $A - \frac{1}{2}a^2|\Psi|^2$ is the entropy deviation decreasing with ordering ($|\Psi|^2 > 0$). Let us consider a one-dimensional steady solution under the following boundary conditions:

$$\begin{aligned} &A \to -1 \qquad \Psi \to (1-k^2)^{1/2}\mathrm{e}^{-\mathrm{i}kx} \qquad (\text{as } x \to -\infty) \\ &A \to \infty \qquad \Psi \to 0 \qquad\qquad\quad (\text{as } x \to \infty). \end{aligned} \tag{3.11}$$

Then (3.9) and (3.10) may be rewritten as

$$\frac{\mathrm{d}^2}{\mathrm{d}x^2}\Psi = \left[-1 + \left(1 - \frac{\mathrm{i}}{a\Gamma}\right)(A+1) + |\Psi|^2 \right] \tag{3.12}$$

$$\frac{\mathrm{d}^2}{\mathrm{d}x^2}A = \mathrm{Re}\left(\frac{1}{\Gamma\lambda}\right)(A+1)|\Psi|^2 \tag{3.13}$$

where $\mathrm{Re}(\cdots)$ denotes taking the real part, and the temperature dependence of λ is neglected. These coupled equations are analogous to those for an interface in type-I superconductors in magnetic fields [49]. In the superconductor case, A is the vector potential and A^2 appears instead of $(1 - \mathrm{i}/ab_1)(A+1)$ in (3.12). The temperature $T - T_\lambda$, temperature gradient ∇T, and heat flow Q in our helium case correspond to the vector potential A, magnetic induction $B = \mathrm{rot}\, A$, and externally applied magnetic field H in the superconductor case, respectively. The relation $T_c - T \propto H$ at the critical magnetic field [49] corresponds to (3.4) in our case, which is the unique relation between Q and $1 - T/T_\lambda$ in steady states.

The above equations cannot be solved analytically. As in the type-I superconductor case [49], a possible analytic method is to introduce a GL parameter κ ($\propto[\mathrm{Re}(1/\Gamma\lambda)]^{-1/2}$) and assume that $\kappa \ll 1$ [5]. In contrast, numerical solutions to the equations are easily obtained. Figure 4 shows two-dimensional simulation results [50], where the side-wall effect is taken into account. To this end we have generalized the model, equations (3.9) and (3.19), to include the normal-fluid velocity $\boldsymbol{v}_n$ which vanishes at the boundary wall, and assume a parabolic profile due to the shear viscosity. In figure 4(a) we can also see a small temperature drop at the cooler end ($x = 0$) which represents the Kapitza resistance.

3.2. Heat flow effects under gravity

Gravity effects can be crucial near T_λ [51, 47], because the transition temperature depends on the pressure and hence on the height as

$$T_\lambda(p) = T_{\lambda top}[1 - Gx] \tag{3.14}$$

where the x-axis is taken in the downward direction, $T_{\lambda top}$ is the transition temperature at the top ($x = 0$), and $G = \rho g|(\partial T/\partial p)_\lambda|/T_\lambda \cong 0.6 \times 10^{-6}$ cm^{-1} on the Earth. Equilibrium two-phase coexistence is realized for the case in which

$$T_{\lambda top} > T > T_{\lambda bot} \tag{3.15}$$

where a superfluid is placed in an upper region and $T_{\lambda bot}$ is the bottom transition temperature. The closeness to the λ-line is represented by the local reduced temperature:

$$\varepsilon = [\ T - T_\lambda(p)\ ]/T_\lambda(p) \cong (T/T_{\lambda top} - 1) + Gx = (T/T_{\lambda bot} - 1) + G(x - L) \tag{3.16}$$

where L is the vertical cell length. The thickness ℓ_g and the typical reduced temperature τ_g of the He I–He II interface are determined by the scaling relations, $\ell_g = \xi_{0-}\tau_g^{-2/3}$ and

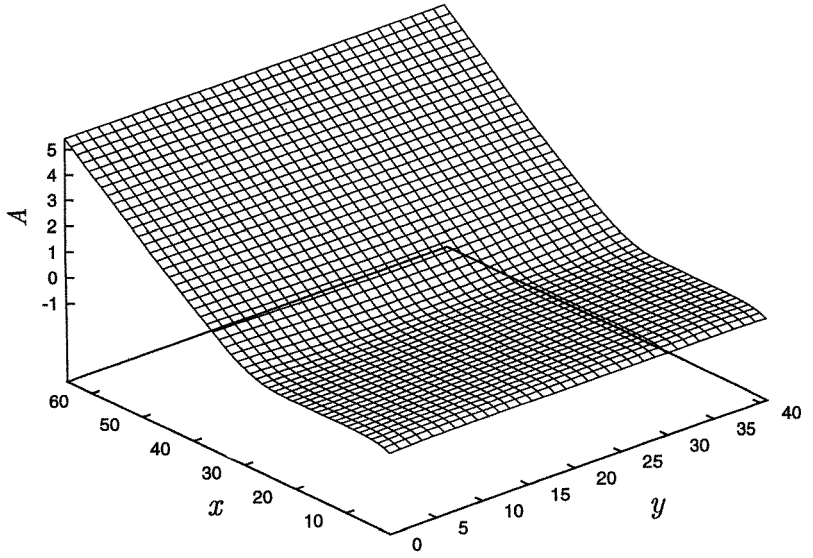

(a)

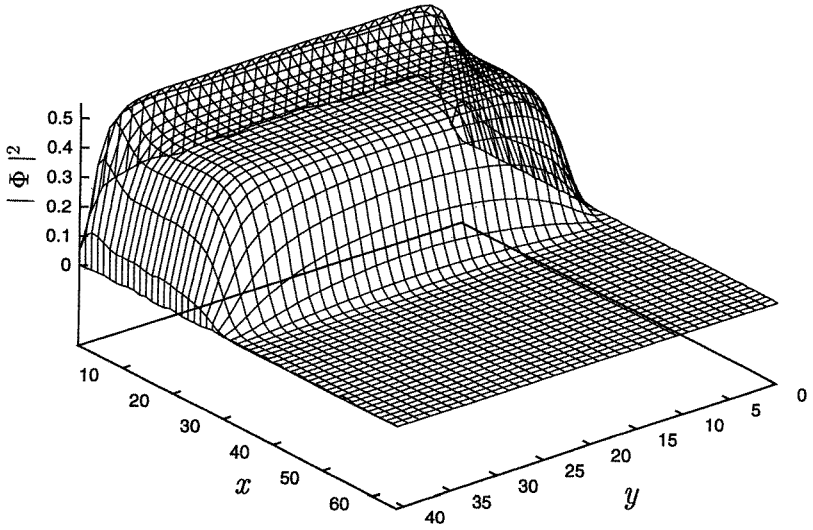

(b)

Figure 4. The temperature profile in (a) and the superfluid density in (b) in two-phase coexistence in ^{4}He. We have assumed a two-dimensional cell, $0 < x < 66$ and $0 < y < 42$. The space is measured in units of the correlation length ξ in the superfluid region. The order parameter Ψ is zero at the boundary walls.

$\tau_g = G\ell_g$, where $\xi_{0-} \sim 1$ Å [47]. These are solved to give

$$\ell_g = \xi_{0-}(\xi_{0-}G)^{-2/5} \tag{3.17}$$

$$\tau_g = (\xi_{0-}G)^{3/5}. \tag{3.18}$$

On the earth we have $\tau_g \sim 10^{-9}$ and $\ell_g \sim 10^{-2}$ cm. It is worth noting that ℓ_g and ξ in (3.5) are comparable for $Q \sim 1$ erg cm^{-2} s^{-1}. At this value of Q, a crossover occurs from

an interface induced by heat flow to that induced by gravity. Space experiments are then needed to enlarge the interface thickness without gravity effects.

Moreover, it has recently been recognized that intriguing nonequilibrium states are realized in the presence of both gravity and heat flow, particularly if ^{4}He is heated from above [6, 52, 53, 9]. Hereafter we discuss two such examples.

3.2.1. The balance of gravity and heat flow in normal-fluid states. We apply a heat flux Q at the top ($x = 0$) in a normal-fluid state. We assume a steady state for simplicity, where the heat conduction equation becomes $\lambda\ \mathrm{d}T/\mathrm{d}x = -Q$. In terms of ε defined by (3.16) we obtain

$$\frac{\mathrm{d}}{\mathrm{d}x}\varepsilon = G - (Q/\lambda^* T_{\lambda 0})\varepsilon^{x_\lambda}. \tag{3.19}$$

Use has been made of (3.1). Remarkably, as x is increased, ε tends to the fixed-point value [6]

$$\varepsilon_c = (\lambda^* T_\lambda G/Q)^{1/x_\lambda} \propto (G/Q)^{2.2} \tag{3.20}$$

exponentially as

$$\varepsilon(x) - \varepsilon_c \propto \exp(-x/\ell_c) \qquad \text{with } \ell_c = \varepsilon_c/(x_\lambda G). \tag{3.21}$$

Here the temperature gradient due to heat flow and the critical temperature gradient due to gravity cancel:

$$\left(\frac{\mathrm{d}}{\mathrm{d}x}T\right)_{\text{heat flow}} = \frac{\mathrm{d}}{\mathrm{d}x}T_\lambda \qquad \text{(in normal fluid)}. \tag{3.22}$$

A sizable bulk region should thus be realizable, in which

$$\varepsilon(x) \cong \varepsilon_c \qquad \lambda \cong Q/T_\lambda G. \tag{3.23}$$

On the Earth, we have

$$\varepsilon_c \cong 2 \times 10^{-9} Q^{-2.2} \qquad \lambda \cong 10^6 Q \qquad \ell_c \cong 4 \times 10^{-3} Q^{-2.2} \tag{3.24}$$

in cgs units.

The approach of ε to ε_c is expected to occur on rather short timescales. In fact, an experiment was performed under slowly evolving transient conditions to confirm the formula (3.20) and the balance (3.22) [9]. See [52, 53] for more arguments on this effect. The normal-fluid state thus realized is in very much a unique nonequilibrium steady state, where the distance to the λ-line can be an extremely small positive constant. In the experiment [9], Q was typically 1 erg cm^{-2} cm^{-1}, which means that the value of $T - T_\lambda(p)$ realized was of order 1 nK. Theoretically we should develop renormalization group theory on this steady state and characterize its stability and critical behaviour.

3.2.2. Vortex generation in a superfluid region expanding from below. In the second example, we prepare a normal-fluid state in equilibrium or heated from above. We then suddenly lower the bottom reduced temperature ε_b to a negative value below a certain critical value to produce an embryo of superfluid at the bottom. The superfluid region continues to grow into the upper normal-fluid region. It will not stop generally if the top temperature is not controlled, but the interface velocity must be very low because a large amount of entropy stored in the normal-fluid region needs to be extracted through the superfluid region. Furthermore, there arises a puzzle: If the temperature is constant in the superfluid region, the reduced temperature ε in (3.16) and hence also the superfluid density

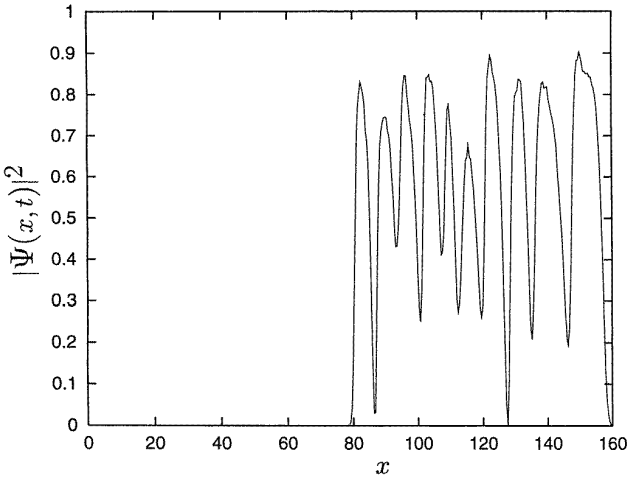

(a)

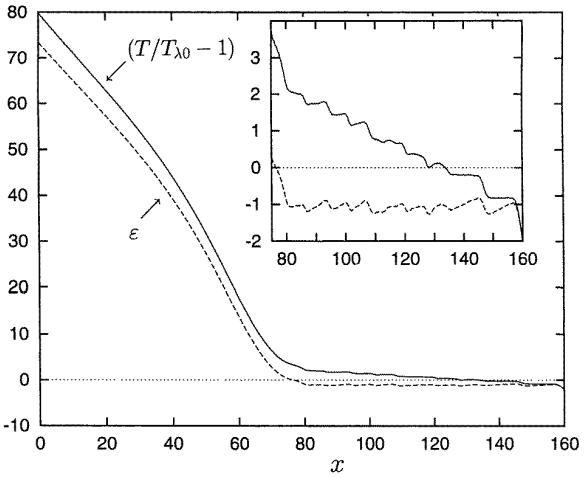

(b)

Figure 5. The superfluid region created at the bottom ($x = 160$) and expanding towards the top ($x = 0$) at $t = 45\,615$. (a) The superfluid density is plotted. There are many phase-slip centres in the expanding superfluid region. The space and time are scaled with respect to 1.54×10^{-3} cm and 10^{-4} s. (b) $T/T_{\lambda bot} - 1$ (solid line) and ε (dashed line) are plotted in the transient state and are expanded in the inset. They are scaled with respect to 2.75×10^{-8}. (c) The heat flux Q scaled with respect to 6.8 erg cm^{-2} s is shown, which arises from the thermal conductivity for $x < 80$ and mostly from the thermal counterflow for $x > 80$.

ρ_s increase with the height, enlarging the entropy difference between the two phases as the interface advances. Another interesting possibility is that vortices are spontaneously created in the superfluid region, which will give rise to a temperature gradient balancing the gravity-induced gradient. That is,

$$\left(\frac{\mathrm{d}}{\mathrm{d}x}T\right)_{\mathrm{vortex}} = \frac{\mathrm{d}}{\mathrm{d}x}T_\lambda \qquad \text{(in expanding superfluid)}. \tag{3.25}$$

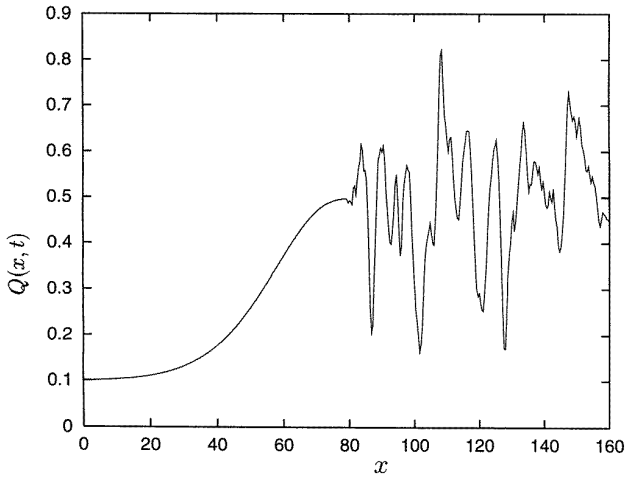

(c)

Figure 5. (Continued)

In our preliminary simulation [52] we have found that the above possibility is in fact the case.

To take into account the gravity effect, we modify (3.9) to

$$\frac{\partial}{\partial t}\Psi = \mathrm{i}a^{-1}A\Psi - \Gamma[\varepsilon\xi^{-1/2} - \nabla^2 + \xi^{-1}|\Psi|^2]\Psi \tag{3.26}$$

where $\varepsilon = A + G(x - L)$ is the reduced temperature (3.16). In the simulation we measure the space, reduced temperature, and heat flow in units of 1.54×10^{-3} cm, 2.75×10^{-8}, and 6.8 erg cm^{-2} s^{-1}, respectively. The unit of time is about 10^{-4} s. Then $G = 0.04$ in these units on the Earth. The local correlation length is defined by $\xi = \ell_g \tanh(\ell_g/|\varepsilon|^{2/3})$, where ℓ_g is given by (3.17). The system is in a normal-fluid state with $\varepsilon_b = 2$, and $Q = 0.1$ for $t < 0$. The top and bottom are at $x = 0$ and $L = 160$, respectively. The bottom reduced temperature ε_b is then lowered to -2 at $t = 0$ with Q held fixed. Figure 5 shows data for $t = 45\,615$: $\rho_s(x,t) = |\Psi(x,t)|^2$ in panel (a), $A(x,t) = T(x,t)/T_{\lambda bot} - 1$ and $\varepsilon(x,t) = T/T_{\lambda bot} - 1 + G(x - L)$ in panel (b), and the heat flux $Q(x,t) = -a\ \mathrm{Im}(\Psi^*\,\partial\Psi/\partial x) - \lambda\,\partial A/\partial x$ in panel (c). Surprisingly, we find a number of phase-slip centres [54], the one-dimensional counterpart of vortices, in (a). They are rapidly varying in time and the temperature (solid line) has a gradient such that ε (dashed line) becomes flat on average in the expanding superfluid region as shown in (b). This confirms the balance (3.25). The heat flux $Q(x,t)$ is shown in (c), which consists mostly of the thermal counterflow in the superfluid region. The heat flux Q_{out} at the bottom is about 0.5, which is five times the heat flux $Q_{in} = Q = 0.1$ at the top. We notice that the superfluid velocity is equal to $Q(x,t)/|\Psi|^2$ and is fluctuating around the critical value $1/\sqrt{3}$ from (c). In the real units this critical value corresponds to $\hbar/\sqrt{3}m$ in (3.3) [43, 44]. For this value of Q_{out}, the time t_{tr} at which the front of the superfluid region reaches the top is estimated in the dimensionless units as

$$t_{tr} \sim L(Q_{in}L)^{1/(1-x_\lambda)}/(Q_{out} - Q_{in}) \tag{3.27}$$

where we assume $Q_{in} = Q \gg 1/L$ and $Q_{out} > Q_{in}$. The time t_{tr} increases dramatically with increasing Q and L.

In our simulation the density of phase-slip centres is very high and is roughly independent of time. Thus the interior of the expanding superfluid region is homogeneous and steady if the irregularities are averaged over the timescale of the phase-slip-centre oscillation. The mechanism producing flat ε is quite different from that of the levelling off of ε in normal-fluid states. In fact, similar flatness still follows in the expanding superfluid region even if we assume that λ is independent of ε. We have performed many similar simulations and found that the formation of dense-phase-slip centres and the flattening of ε occur over wide ranges of Q, ε_b, and the coefficients in the model. Furthermore, we may easily perform the above calculation in two dimensions as in reference [50] and have already confirmed the emergence of a number of vortices and the same flattening of ε in the expanding superfluid region.

In one dimension we have also found that the superfluid velocity v_s is fluctuating around the critical superfluid velocity v_{sc} in (3.3). The previous theories [43, 44, 5, 8] neglect vortices and predict an instability analogous to spinodal decomposition where long-wavelength fluctuations of the order parameter grow above v_{sc} . The correct singular objects produced by the instability are phase-slip centres in one dimension and are apparently vortices in higher dimensions. Notice that vortices are known to appear via the nucleation mechanism at a much smaller critical superfluid velocity v_{sn} of order $0.0036\overline{h}/m\xi$ [46]. We should distinguish between the two critical velocities, v_{sc} and v_{sn}, because the mechanisms involved are very different. There has been no experiment near the λ-point in which v_{sc} is exceeded.

Can we expect the same bulk instability and encounter high-density vortices in an expanding superfluid region in experiments? Do they produce a temperature gradient equal to $\mathrm{d}T_\lambda/\mathrm{d}x$? Note that, if a superfluid state is not very close to the λ-point and is exposed to a much larger heat flux, the usual mutual friction can give rise to a larger temperature gradient. One such example, where the gravity effect is negligible, namely Ahlers' result [55] for $T_\lambda - T \gtrsim 10^{-4}$ K, may be rewritten as

$$\left(\frac{\mathrm{d}}{\mathrm{d}x}T\right)_{\mathrm{gravity-free}} = 5\times 10^{-29} T_\lambda |\varepsilon|^{-2.23} Q^3 \tag{3.28}$$

with Q in erg cm^{-2} s^{-1}. In gravity-free conditions in space, this temperature gradient will be measured even extremely close to T_λ. By requiring that this gradient is smaller than GT_λ, we obtain $Q/Q_0 < 8|\varepsilon/\varepsilon_0|^{0.75}$, where $\varepsilon_0 = 2.75\times 10^{-8}$ and $Q_0 = 6.8$ erg cm^{-2} s^{-1} are the units in our simulations. This condition is satisfied for $Q(x,t)$ in figure 5(c) and was not in reference [55]. Furthermore, by setting $v_s \sim \overline{h}/\sqrt{3}m\xi$ and removing Q, we obtain the condition on the bottom reduced temperature

$$|\varepsilon_b| = 1 - T/T_{\lambda bot} \lesssim 10^{-5} \tag{3.29}$$

under which the Earth's gravity serves to appreciably increase the vortex line density.

4. Summary

We have clarified the mechanisms of the shear flow effects in three very different fluids.

(i) In near-critical fluids, the effect arises from flow-induced deformations taking place on the timescale of S^{-1}. The nonlinear hydrodynamic interaction is suppressed, leading to a downward shift of the critical temperature.

(ii) In semidilute polymer solutions in theta solvent, composition fluctuations induce heterogeneous stress imbalance, leading to diffusion in the direction of segregation even

above the coexistence curve. But phase separation takes place only incompletely due to the flow-induced deformations. Here the heterogeneities can reduce the shear stress and in this sense the effect is thermomechanical.

(iii) Highly supercooled liquids are characterized by a slow thermal activation time τ_α in quiescent states. If we apply shear flow with $S\tau_\alpha > 1$, structural relaxations take place in the form of shear-induced jump motions on the timescale of $1/S$, thus giving rise to a new nonlinear response regime. Here even a very small shear can greatly accelerate *microscopic* rearrangement processes. This effect is also the origin of the highly ductile properties of amorphous metals [38–40]. Large-scale molecular dynamics simulations away from equilibrium should be of utmost importance for understanding such unsolved but technologically important problems in the future.

We also the apply heat flow Q to ^{4}He near the superfluid transition, which is extremely sensitive to heat flow and gravity very close to the λ-point.

(i) As is well known, this brings about the coexistence of a superfluid region and a normal-fluid region separated by a thin interface with thickness proportional to $Q^{-1/2}$.

(ii) When ^{4}He is heated from above in a normal-fluid state, the temperature gradient due to the finite thermal conductivity can balance with the transition temperature gradient under gravity, leading to a homogeneous steady state with a constant reduced temperature $T - T_\lambda(p)$.

(iii) When a normal-fluid state is cooled from the bottom below the transition, a superfluid region appears at the bottom and slowly expands in the upward direction. If the bottom temperature T_b is close to the bottom transition temperature $T_{\lambda bot}$ ($T_{\lambda bot} - T_b \lesssim 10^{-5}$ K), the superfluid velocity in the expanding superfluid region approaches a maximum, leading to dense generation of vortices. The temperature gradient due to such vortices balances with the transition temperature gradient under gravity. Experiments in this direction should be exciting.

References

[1] Onuki A 1987 *J. Phys. C: Solid State Phys.* **9** 6119
[2] Yamamoto R and Onuki A 1997 *J. Phys. Soc. Japan* **66** 2545
[3] Yamamoto R and Onuki A 1997 *Europhys. Lett.* **40** 61
Yamamoto R and Onuki A 1997 *Phys. Rev.* E **58** 3515
[4] Onuki A and Yamamoto R 1998 *J. Non-Cryst. Solids* **235–237** 34
[5] Onuki A 1983 *J. Low Temp. Phys.* **50** 433
Onuki A 1984 *J. Low Temp. Phys.* **55** 309
[6] Onuki A 1987 *Proc. 18th Int. Conf. on Low Temperature Physics; Japan. J. Appl. Phys.* **26** 365
[7] Duncan R V, Ahlers G and Steinberg V 1988 *Phys. Rev. Lett.* **60** 1522
Ahlers G and Duncan R V 1990 *Frontiers of Physics, Proc. of the Landau Memorial Conf. (Tel Aviv, 1988)* ed E Gotsman, Y Ne'eman and A Voronel (Oxford: Pergamon) p 219
[8] Haussmann R and Dohm V 1992 *Phys. Rev.* B **46** 6361
[9] Moeur W A, Day P K, Liu F-C, Boyd S T P, Adriaans M J and Duncan R V 1997 *Phys. Rev. Lett.* **78** 2421
[10] Onuki A and Kawasaki K 1979 *Ann. Phys., NY* **121** 456
Onuki A, Yamazaki K and Kawasaki K 1981 *Ann. Phys., NY* **131** 217
[11] Beysens D and Gbadamassi M *Phys. Rev.* A **22** 2250
Beysens D, Gbadamassi M and Moncef-Bouanz B 1983 *Phys. Rev.* A **28** 2491
[12] Pine D J, Eswar N, Maher J V and Goldburg W I 1984 *Phys. Rev.* A **29** 308
[13] Chan C K and Goldburg W I 1987 *Phys. Rev.* A **35** 1756
[14] Tong P, Goldburg W I, Stavans J and Onuki A 1989 *Phys. Rev. Lett.* **62** 2472
[15] Larson R G 1992 *Rheol. Acta* **31** 497
[16] Wu X L, Pine D J and Dixon P K 1991 *Phys. Rev. Lett.* **68** 2408
[17] Hashimoto T and Fujioka K 1991 *J. Phys. Soc. Japan* **60** 356

Hashimoto T and Kume T 1992 *J. Phys. Soc. Japan* **61** 1839
Murase H, Kume T, Hashimoto T, Ohta Y and Mizukami T 1995 *Macromolecules* **28** 7724
[18] van Egmond J, Werner D E and Fuller G G 1992 *J. Chem. Phys.* **96** 7742
[19] Nakatani A I, Douglas J F, Ban Y-B and Han C C 1994 *J. Chem. Phys.* **100** 3224
[20] Brochard F and de Gennes P G 1977 *Macromolecules* **10** 1157
[21] Tanaka T, Hocker L O and Benedik G B 1973 *J. Chem. Phys.* **59** 5151
[22] Helfand E and Fredrickson H 1989 *Phys. Rev. Lett.* **62** 2468
[23] Onuki A 1990 *J. Phys. Soc. Japan* **59** 3423
Onuki A 1990 *J. Phys. Soc. Japan* **59** 3427
[24] Doi M and Onuki A 1992 *J. Physique* II **2** 1631
[25] Milner S T 1993 *Phys. Rev.* E **48** 3874
[26] Onuki A, Yamamoto R and Taniguchi T 1997 *J. Physique* II **7** 295
Onuki A, Yamamoto R and Taniguchi T 1997 *Prog. Colloid Polym. Sci.* **106** 150
[27] Tanaka H 1993 *Phys. Rev. Lett.* **71** 3158
Tanaka H 1994 *J. Chem. Phys.* **100** 5253
[28] Onuki A and Taniguchi T 1997 *J. Chem. Phys.* **106** 5761
[29] Ediger M D, Angell C A and Nagel S R 1996 *J. Phys. Chem.* **100** 13 200
[30] Adam G and Gibbs J H 1965 *J. Chem. Phys.* **43** 139
[31] Muranaka T and Hiwatari Y 1997 *Prog. Theor. Phys. Suppl.* **126** 403
[32] Hurley M M and Harrowell P 1995 *Phys. Rev.* E **52** 1694
Perera D N and Harrowell P 1996 *Phys. Rev.* E **54** 1652
[33] Simmons J H, Ochoa R, Simmons K D and Mills J J 1988 *J. Non-Cryst. Solids* **105** 313
[34] Okuzono T and Kawasaki K 1995 *Phys. Rev.* E **51** 1246
[35] Durian J D 1997 *Phys. Rev.* E **55** 1739
[36] Langer S A and Liu A J 1997 *J. Phys. Chem.* B **101** 8667
[37] Miller B, O'Hern C and Behringer R P 1996 *Phys. Rev. Lett.* **77** 3110
[38] Spaepen F 1977 *Acta Metall.* **25** 407
[39] Aragon A S 1979 *Acta Metall.* **27** 47
[40] Maeda K and Takeuchi S 1978 *Phys. Status Solidi* **49** 685
Kobayashi S, Maeda K and Takeuchi S 1980 *Acta Metall.* **28** 1641
Maeda K and Takeuchi S 1981 *Phil. Mag.* A **44** 643
[41] Tam W Y and Ahlers G 1982 *Phys. Rev.* B **32** 5932
[42] Dingus M, Zhong F and Meyer H 1996 *J. Low Temp. Phys.* **65** 185
[43] Mikeska H J 1969 *Phys. Rev.* **179** 166
[44] Kramer L 1969 *Phys. Rev.* **179** 149
[45] Kramer L and Zimmermann W 1985 *Physica* D **16** 221
[46] Clow J R and Reppy J D 1967 *Phys. Rev. Lett.* **19** 291
[47] Ginzburg V L and Sobaynin A A 1976 *Usp. Fiz. Nauk* **120** 153 (Engl. Transl. 1976 *Sov. Phys.–Usp.* **19** 773)
[48] Halperin B I, Hohenberg P C and Siggia E D 1976 *Phys. Rev.* B **13** 1299
[49] Ginzburg V L and Landau L D 1950 *Zh. Eksp. Teor. Fiz.* **20** 1064
[50] Onuki A and Yamazaki Y 1996 *J. Low Temp. Phys.* **103** 131
[51] Ahlers G 1968 *Phys. Rev.* **171** 275
[52] Onuki A 1996 *J. Low Temp. Phys.* **104** 133
[53] Ahlers G and Liu F-C 1996 *J. Low Temp. Phys.* **105** 255
[54] Langer J S and Ambegaokar V 1967 *Phys. Rev.* **164** 498
[55] Ahlers G 1969 *Phys. Rev. Lett.* **22** 54